PROCEEDINGS OF SPIE

SPIEDigitalLibrary.org/conference-proceedings-of-spie

Aberration correction for hard x-ray focusing at the nanoscale

Frank Seiboth
Andreas Schropp
Maria Scholz
Felix Wittwer
Christian Rödel
Martin Wünsche
Tobias Ullsperger
Stefan Nolte
Jussi Rahomäki
Karolis Parfeniukas
Stylianos Giakoumidis
Ulrich Vogt
Ulrich Wagner
Christoph Rau
Ulrike Boesenberg
Jan Garrevoet
Gerald Falkenberg
Eric C. Galtier

SPIE.

Aberration Correction for Hard X-ray Focusing at the Nanoscale

Frank Seiboth[a,b], Andreas Schropp[a], Maria Scholz[a], Felix Wittwer[a], Christian Rödel[b,c], Martin Wünsche[c], Tobias Ullsperger[d], Stefan Nolte[d], Jussi Rahomäki[e], Karolis Parfeniukas[e], Stylianos Giakoumidis[e], Ulrich Vogt[e], Ulrich Wagner[f], Christoph Rau[f], Ulrike Boesenberg[a], Jan Garrevoet[a], Gerald Falkenberg[a], Eric C. Galtier[b], Hae Ja Lee[b], Bob Nagler[b], and Christian G. Schroer[a,g]

[a]Deutsches Elektronen-Synchrotron DESY, Notkestr. 85, 22607 Hamburg, Germany
[b]Linac Coherent Light Source, SLAC National Accelerator Laboratory, 2575 Sand Hill Road, 94025 Menlo Park, CA, USA
[c]Institute of Optics and Quantum Electronics, Friedrich-Schiller-Universität Jena, Max-Wien-Platz 1, 07743 Jena, Germany
[d]Institute of Applied Physics, Friedrich-Schiller-Universität Jena, Albert-Einstein-Str. 15, 07745 Jena, Germany
[e]KTH Royal Institute of Technology, Biomedical and X-ray Physics, Albanova University Center, 106 91 Stockholm, Sweden
[f]Diamond Light Source Ltd, Diamond House, Harwell Science and Innovation Campus, Didcot, Oxfordshire OX11 0DE, United Kingdom
[g]Department Physik, Universität Hamburg, Luruper Chaussee 149, 22761 Hamburg, Germany

ABSTRACT

We developed a corrective phase plate that enables the correction of residual aberration in reflective, diffractive, and refractive X-ray optics. The principle is demonstrated on a stack of beryllium compound refractive lenses with a numerical aperture of 0.49×10^{-3} at three different synchrotron radiation and x-ray free-electron laser facilities. By introducing this phase plate into the beam path, we were able to correct the spherical aberration of the optical system and improve the Strehl ratio of the optics from 0.29(7) to 0.87(5), creating a diffraction-limited, large aperture, nanofocusing optics that is radiation resistant and very compact.

Keywords: x-ray optics, compound refractive lenses, aberration correction, ptychography, wavefront sensing

1. INTRODUCTION

With the increasing number of operational X-ray free-electron lasers[1] (XFELs) and upcoming ultra-low emittance storage ring sources[2] an increasing demand for radiation resistant and high-performing X-ray focusing optics exists. The creation of small and intense focal spots is essential to confine the beam and concentrate the radiation on the sample. By maximizing the intensity and spatial resolution at the same time new research opportunities in nonlinear X-ray physics,[3] high-resolution imaging[4] and crystallography[5] are enabled. While tight focusing at the nanoscale is routinely achieved at current storage ring sources with diffractive,[6] refractive,[7] and reflective optics,[8] only a few of them are suited for operation at these new and upcoming X-ray sources. The most demanding requirements are radiation resistance while also providing a large aperture to capture the full X-ray beam. So far, mainly mirror systems[9,10] and beryllium compound refractive lenses[11,12] (Be CRLs) are in routine operation at XFELs. Owing to the short X-ray wavelength the fabrication of optics requires the most advanced technologies to achieve the required structure sizes and fulfill the high demands on figure error and

Further author information: (Send correspondence to Frank Seiboth)
Frank Seiboth: E-mail: frank.seiboth@desy.de, Telephone: +1 (650) 926-2048

Advances in X-Ray/EUV Optics and Components XII, edited by Christian Morawe, Ali M. Khounsary, Shunji Goto, Proc. of SPIE Vol. 10386, 103860A · © 2017 SPIE
CCC code: 0277-786X/17/$18 · doi: 10.1117/12.2274030

surface quality. Today, most X-ray optics are limited by high manufacturing requirements when high numerical apertures (NA) are demanded, introducing aberrations to the optical system.

Here, we present the correction of residual spherical aberration in a stack of Be CRLs with $NA = 0.49 \times 10^{-3}$ by a phase plate that is made to measure for these optics. Since the phase plate operates in transmission and is based on refraction, it is largely insensitive to shape and surface inaccuracies on the order of a few µm. Hence, it can correct not only accumulated surface error in large CRL stacks as shown here, but also zone deformations of diffractive optics and figure errors of reflective optics.

2. WAVEFIELD CHARACTERIZATION BY PTYCHOGRAPHY

Scanning coherent X-ray diffraction imaging, known as ptychography,[13] has become a widely used tool not only for imaging extended objects at the nanoscale, but also to determine the wavefield generated by X-ray optics.[14–17] Thus, the method allows to thoroughly characterize these components and guides the design of enhanced optics[18–20] and corrective elements[21] to further improve the optical performance towards diffraction-limited X-ray optics with highest NA.

Here, we characterized the wavefield at the exit of a stack of 20 Be CRLs. The lens stacks were assembled randomly from a pool of 50 lenses and employed at three different sites: beamline I13-1[22] of Diamond Light Source (DLS), the Matter in Extreme Conditions instrument (MEC)[23] at the Linac Coherent Light Source (LCLS), and beamline P06[24] at PETRA III (cf. Table 1). For all experiments the X-rays were monochromatized by a Si-111 monochromator to an X-ray energy of $E = 8.2\,\mathrm{keV}$. The optics aperture was defined by a pinhole with $D = 300\,\mu\mathrm{m}$ diameter. With a given radius of curvature of $R = 50\,\mu\mathrm{m}$ for the lenses the focal length is $f = 250\,\mathrm{mm}$ with $NA = 0.49 \times 10^{-3}$ and a nominal diffraction-limited spot size of 143 nm. The test sample, an array of small Siemens stars structured into 1 µm thick tungsten on a diamond substrate, was placed in the vicinity of the focal plane, as shown in Fig. 1.

For beam characterization the sample was raster scanned on a grid along the x and y direction. Far-field diffraction patterns were recorded using a Merlin detector positioned[25] 2.62 m behind the sample (at DLS), a LAMBDA detector[26] positioned 2.19 m after the sample (at PETRA III), and a CS-PAD 140k detector[27] at a distance of 4.8 m downstream the sample (at LCLS). For each ptychographic data set we considered roughly 400 diffraction patterns, covering an area of $2\,\mu\mathrm{m} \times 2\,\mu\mathrm{m}$ on the sample. Data at the storage ring facilities DLS and PETRA III was recorded in a step scanning mode, taking one far-field image per step. The acquisition time per point was 1 s at DLS and 2 s at PETRA III.

Data at the LCLS was collected in a fly-scanning mode along the y direction. While moving with a constant velocity of $1.2\,\mu\mathrm{m\,s}^{-1}$ we collected 203 diffraction patterns per line, covering a distance of roughly 2 µm and operating at 120 Hz repetition rate. After a single line was finished, the sample was moved by 100 nm in x direction and a new continuous acquisition cycle began. A complete scan was recorded within 60 s. From the 4060 diffraction patterns per scan we discarded shots with low pulse energy and also shots that overexposed the camera. The beam was attenuated to avoid radiation damage to the sample. Due to the extremely short X-ray pulse duration of 50 fs the sample is frozen in space during each exposure. Thus, we did not employ a sophisticated reconstruction algorithm accounting for incoherence due to sample movement during exposure,[28–30] but could use a simple ePIE algorithm[31] with iterative position refinement[11,32] for data collected at all facilities.

3. SPHERICAL ABERRATION OF BERYLLIUM LENSES

While refractive optics inherently exhibit chromatic aberration, shape deviations from the ideal parabolic thickness profile of these lenses can lead to various other types of aberration. As Be CRLs are made by a coining process where the shape is defined by a molding tool made on a turning lathe under constant rotation, their shape is also rotational symmetric. The same goes for profile errors originating from shape errors of the molding tool. Hence, the predominant type of aberrations in these optics is spherical aberration.[11,34] As many CRLs are typically stacked to form a lens with short focal length and high NA, shape errors add up and aberrations become severe for CRL optics with higher $NA \geq 0.5 \times 10^{-3}$. For an individual lens surface of the CRLs used here ($R = 50\,\mu\mathrm{m}$) it was found that the shape only deviates by 0.5 µm from the ideal parabola over the whole lens aperture of $D = 300\,\mu\mathrm{m}$.[21] As the shape deviation of the molding tool associated with these resulting lens errors

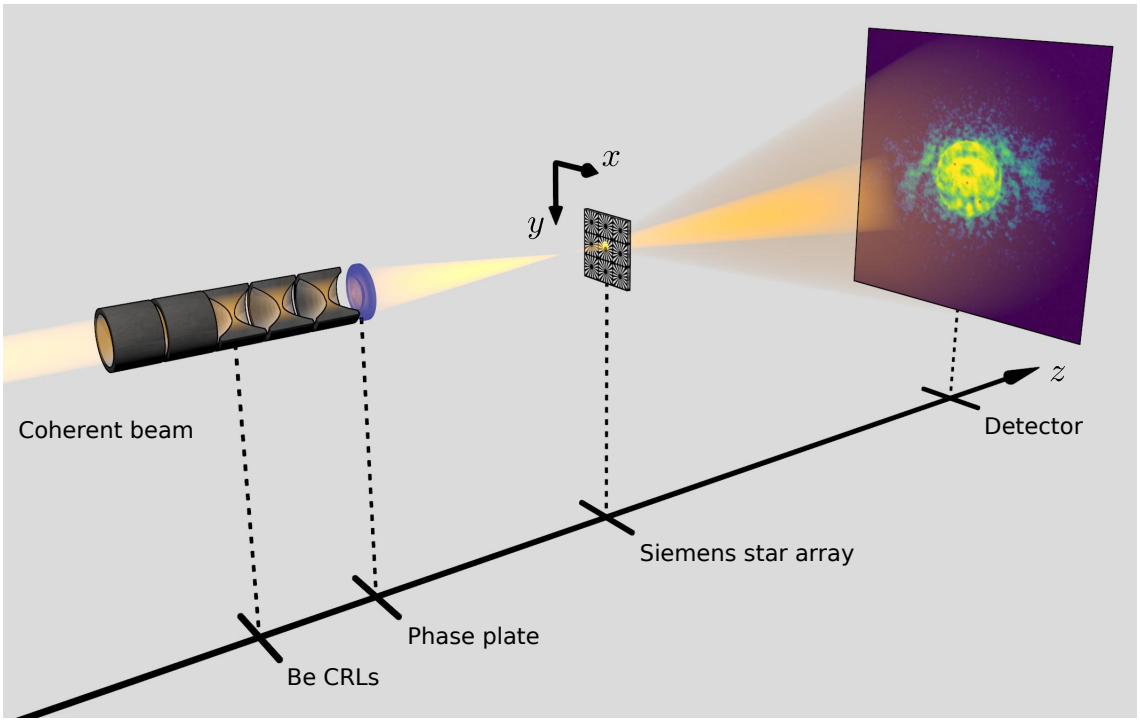

Figure 1. Schematic of the experimental setup. The coherent X-ray beam was confined to the lens aperture with a pinhole of 300 µm diameter. The lens, a stack of 20 Be-CRLs with radius of curvature of 50 µm was used to focus the beam at a focal distance of 250 mm. A corrective phase plate was positioned after the lens stack. The test sample was placed in the vicinity of the focal plane and scanned on a grid along the x and y direction. Far-field diffraction patterns were recorded with different area detectors at each facility.

is at the very limit of the precision of current turning lathes used to fabricate the mold, an improvement on the shape of individual lenses is very challenging. Instead, a corrective phase plate was designed and manufactured to correct the accumulated phase error in larger lens stacks.[21]

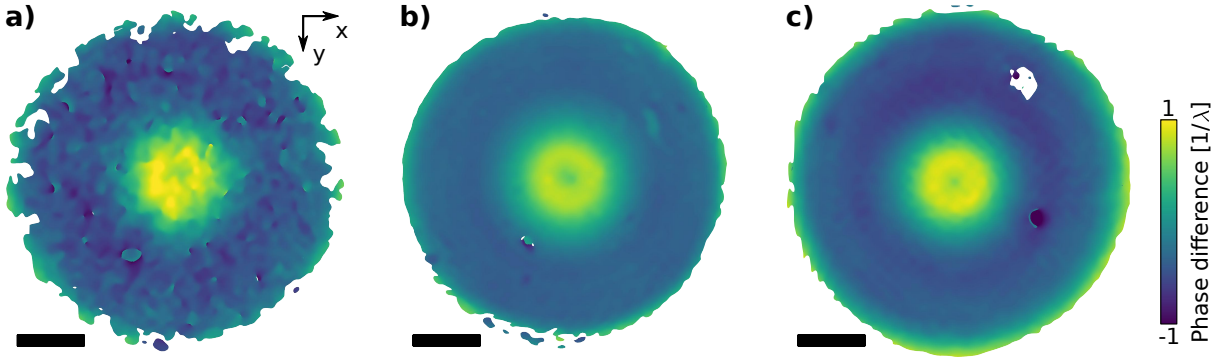

Figure 2. Recovered wavefield error compared to a perfect spherical wave (a, b, c) for data sets #1, #3, and #5, respectively (cf. Table 1). The wavefields are recovered in the plane where the phase plate will be installed later on (cf. Fig. 1). All scale bars represent 50 µm and the color scale is the same for all sub figures.

Here, we have assembled three different lens stacks at three synchrotron radiation and XFEL facilities (cf. Table 1) and measured the wavefield behind these optics in the vicinity of the focal plane by ptychography. The retrieved complex valued probe function at the sample position Ψ_p was propagated by a distance $-\Delta z$ upstream

Table 1. Summarized results quantifying wavefront errors for aberrated and aberration-corrected Be CRL stacks ($N = 20$, $R = 50\,\mu\text{m}$) at the three facilities. The optical performance is investigated in terms of relative intensity in the focal plane compared to an aberration-free lens, the root-mean-square error $\Delta\varphi_\sigma$ and peak-to-valley error $\Delta\varphi_{\text{PV}}$ of the wavefield at the phase plate position, and the sum of the absolute values for the Zernike coefficients $\sum|z_{\text{sph}}|$ representing spherical aberration (z_4^0, z_6^0, z_8^0).

#	Facility	Phase plate	Rel. peak intensity		$\Delta\varphi_\sigma$ [λ^{-1}]	$\Delta\varphi_{\text{PV}}$ [λ^{-1}]	$\sum\|z_{\text{sph}}\|$ [λ^{-1}]
			speckle‡	on axis§			
1	DLS I13	-	0.16	0.24	0.32	2.02	0.45
2		PP1, +15 mm*	0.72	0.94	0.08	1.21	0.09
3	LCLS MEC	-	0.30	0.39	0.23	1.51	0.33
4		PP1, +20 mm*	0.83	0.87	0.06	1.06	0.06
5	PETRA III P06	-	0.22	0.23	0.33	2.31	0.48
6		PP2, +0 mm†	0.85	0.81	0.07	0.87	0.04

*Mounted downstream outside of lens holder, adjustable in x and y.

†Fixed mounting position directly after lens stack within CRL holder.

‡Integrated intensity in central speckle, relative to aberration-free lens.

§On optical axis (maximum of Gaussian fit), relative to aberration-free lens (corresponds to Strehl ratio[33]).

to the prospective phase plate position $\Psi_{\text{PP}} = \mathcal{K}_{-\Delta z}\Psi_p$ using the Fresnel-Kirchhoff diffraction integral[35] with the propagation operator

$$(\mathcal{K}_{\Delta z}\bullet)(x,y) = \iint_{-\infty}^{+\infty} \bullet(\zeta,\eta) K_{\Delta z}(x-\zeta, y-\eta)\, d\zeta\, d\eta$$

and the kernel

$$K_{\Delta z}(x,y) = -\frac{\mathrm{i}k}{4\pi}\frac{e^{\mathrm{i}k\Delta z}}{\Delta z} e^{\frac{\mathrm{i}k}{2\Delta z}(x^2+y^2)} \,.$$

From the wavefield Ψ_{PP} we can reveal wavefront errors Ψ_ϵ by subtracting the phase of a spherical wave $\varphi_{\Delta z_f}(x,y) = -k\left(\sqrt{\Delta z^2 + x^2 + y^2} - \Delta z_f\right)$ with radius z_f, corresponding to the distance from the phase plate plane Ψ_{PP} to the focus position:

$$\Psi_\epsilon = \Psi_{\text{PP}} e^{\mathrm{i}\varphi_{\Delta z_f}(x,y)} \,.$$

The recovered phase deviation Ψ_ϵ for the Be CRL optics alone is shown in Fig. 2. For data set #1 shown in Fig. 2a the algorithm struggled to reconstruct the amplitudes, leading to false phase information in areas with low amplitudes, which explains the patchy appearance in the phases. If both the phases and amplitudes are recovered well, the wavefield is smooth and the phase continuous over the whole lens aperture (cf. Fig. 2b,c). Despite the difficult phase retrieval shown in Fig. 2a, Zernike polynomials can be fitted[36] to all data in Fig. 2 and the strength of various types of aberrations can be extracted (cf. Table 1 and Fig. 5). As each experiment was performed with a different stack of lenses, the wavefield deformation and strength of spherical aberration, represented by z_4^0, z_6^0, and z_8^0 in Fig. 5 and $\sum|z_{\text{sph}}|$ in Table 1, varied slightly.

To correct for these wavefield deformations a phase plate can be designed to compensate the observed phase error by inducing an opposing phase shift.[21] For best results the phase plate has to be fitted to the individual lens configuration of the experiment. Here, the shape of the phase plate is based upon the aberration measured by Schropp et al.[11] and is described in more detail in the following Section 4.

4. FUSED SILICA PHASE PLATES

In order to achieve a good correction of residual wavefield errors the compensating phase plate has to be matched to the specific optics and also used at the designed position along the optical axis. As the beam for high NA optics converges significantly, the derived shape of a phase plate is only matching to the wavefront at a distinct

position. For the initial design of the phase plate we decided to place it directly behind the lens stack, positioned in a casing very similar to the ones used for Be CRLs. In this way the phase plate can be mounted in conjunction with the Be CRLs within the same holder and no further alignment is necessary.

To retrieve the thickness profile $z_{\mathrm{PP}}(x, y)$ for the phase plate, detailed knowledge of phase errors at that position is needed (cf. Fig. 2). Based upon the retrieved probe function Ψ_p from Schropp et al.[11] we calculated Ψ_ϵ at the phase plate position. As the induced phase shift of the phase plate $\varphi_{\mathrm{PP}}(x, y) = -k\delta_{\mathrm{SiO_2}} z_{\mathrm{PP}}(x, y)$ shall compensate the phase deviations in Ψ_ϵ, i. e. $\arg \Psi_\epsilon = -\varphi_{\mathrm{PP}}$, the profile is given by

$$z_{\mathrm{PP}}(x, y) = \frac{\arg\left[\Psi_\epsilon(x, y)\right]}{k\delta_{\mathrm{SiO_2}}} \,.$$

The retrieved shape was structured via laser micromachining into an amorphous SiO_2 substrate (Vitreosil 077, $\rho = 2.2\,\mathrm{g\,cm^{-3}}$) with a thickness of 118(2) µm. For ablating the substrate surface we used the Trumpf TruMicro 5050 ultrashort-pulsed laser system. A microscope objective with $NA = 0.4$ served to focus the pulses onto the substrate, providing a spot size of 1 µm and enabling nonlinear absorption in the focal region for highly localized energy transfer.[37,38] The laser emits pulses of 8 ps duration at a wavelength of 1030 nm. The pulse energy was set to 0.2 µJ in order to guarantee precise ablation of the desired structure. As Be CRLs are rotational symmetric we enforced the same geometry on the phase plate. During fabrication the substrate was moved on a spiral trajectory going from the optical axis outwards with constant velocity. With each pass a layer of 1 µm was ablated. The resulting profiles are shown in Fig. 3. A line scan across the two-dimensional thickness profile in Fig. 3a is plotted in Fig. 3b for three phase plates. The two phase plates used during experiments (PP1 and PP2, cf. Table 1) match the desired shape (dashed red line) well, but deviate in some areas due to fluctuations in the ablation process. However, the profile can be reproduced with high accuracy if the process is stable (gray dotted line). The fabricated phase plates transmit roughly 54 % for 8.2 keV X-rays owing to absorption of the substrate material. A thinner substrate would allow for higher transmission.

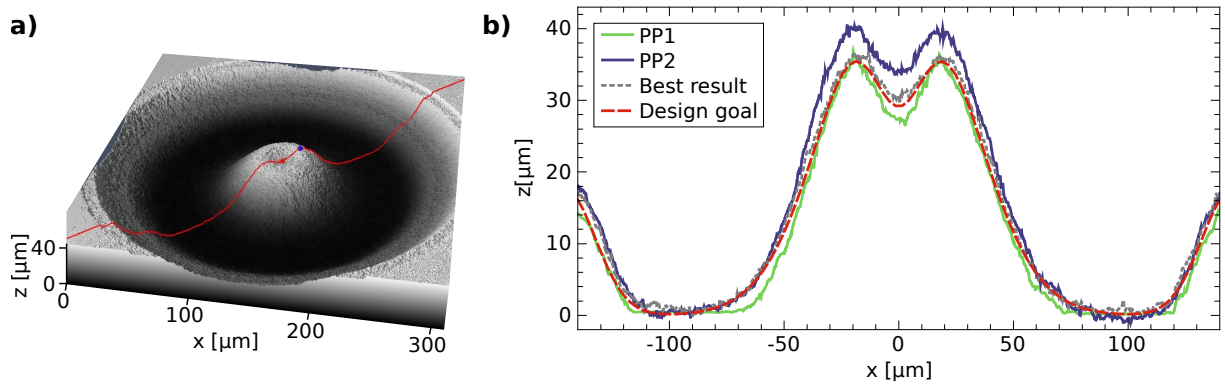

Figure 3. Surface profile of phase plates manufactured out of fused silica. (a) Two-dimensional profile measured by a laser scanning microscope. (b) Line scans across the measured profile [red line in (a)] for various phase plates compared to the design goal.

5. ABERRATION-CORRECTED BERYLLIUM LENSES

For best possible aberration correction the phase plate needs to be positioned not only at the right spot along the optical axis, but the lateral alignment is crucial. Here, an accuracy of ≤ 2 µm is required to achieve diffraction-limited performance for the whole optical system. Mounting a phase plate within these tolerances into the center of a casing with 12 mm diameter (standard Be CRL casing diameter) is not trivial. As the first produced phase plate, labeled PP1, was not centered well, we had to mount it outside the lens holder to be able to align the phase plate in the x-y plane with respect to the Be CRL lens within the required tolerances. As a result, the phase plate could not be placed at the designed location directly after the lens, but was positioned 15 mm and 20 mm downstream of the lens exit for the experiments at DLS and LCLS, respectively (cf. Table 1). For alignment,

we relied on the Ronchi test[39] to provide an immediate and qualitative feedback on present aberrations on a single exposure or single shot basis. After this initial alignment, the wavefield in the vicinity of the focal plane was measured again by ptychography. Subsequently, the wavefield was backpropagated into the same plane as shown for the aberrated lenses in Fig. 2. The corrected wavefields for PP1 employed at DLS and LCLS are shown in Figs. 4a and 4b, respectively. For the second phase plate, called PP2, the initial alignment with the casing was good enough in order to directly mount PP2 after the Be CRL stack within the holder. Thus, the phase plate required no special alignment and could be integrated in a very compact way within the lens stack. The corresponding data was recorded at PETRA III (cf. Table 1) and the remaining wavefront errors after phase plate correction are shown in Fig. 4c. As the data in Fig. 4 are on the same color scale as in Fig. 2, the reduction in wavefront errors is immediately visible, particularly in the center of the wavefield around the optical axis. The standard deviation compared to a perfect sphere $\Delta\varphi_\sigma$ was reduced from over $0.23\,\lambda^{-1}$ to well below $0.08\,\lambda^{-1}$. The peak-to-valley error $\Delta\varphi_{\mathrm{PV}}$ is mostly dominated by deviations near the edge of the optics aperture or in areas of very low amplitude and impurities, e. g., the small dark blue spot visible in all images shown in Fig. 4. Nevertheless, $\Delta\varphi_{\mathrm{PV}}$ was reduced significantly in all cases, summarized in Table 1.

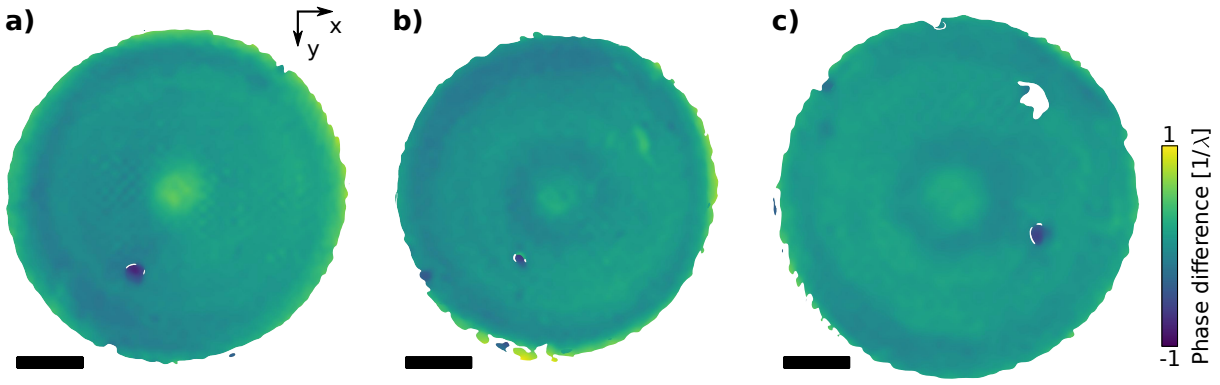

Figure 4. Recovered wavefield error with the corrective phase plate installed compared to a perfect spherical wave in the plane of the phase plate (a, b, c) for data sets #2, #4, and #6, respectively (cf. Table 1). All scale bars represent 50 µm and the color scale is the same for all sub figures.

To quantitatively compare the strength of different aberration types for the Be CRLs alone (cf. Fig. 2) and after correction with a phase plate (cf. Fig. 4) the first 37 Zernike polynomials were fitted to the retrieved wavefields.[36] The resulting amplitudes z_n^m of relevant Zernike polynomials Z_n^m are shown in Fig. 5 for all experiments. The diagrams show that also tilt errors are present, especially in Fig. 5a in x direction (z_1^1) and Fig. 5c in y direction (z_1^{-1}). Main reason for these initial tilts is the discrete pixel size of the diffraction patterns. If the center of the diffraction pattern is not exactly in the center of a single pixel, a slight tilt is introduced into the reconstructed wavefield to compensate for the off-centered optical axis. When introducing the phase plate into the optical system the tilt error changed, getting more pronounced for DLS and LCLS, represented by Figs. 5a and 5b, respectively. Depending on the centering of the phase plate with respect to the optical axis a slight misalignment can introduce an additional tilt. In general, Zernike coefficients representing astigmatism, coma, and trefoil are very small. As the phase plate is rotationally symmetric no changes for these aberration types were expected and the data shown in Fig. 5 confirm this. The primary spherical aberration z_4^0 and their higher orders z_6^0 and z_8^0 on the other hand could be reduced drastically in all cases. The total strength of spherical aberration $|z_4^0| + |z_6^0| + |z_8^0|$ is summarized in Table 1.

An important measure for scanning microscopy applications is the focal spot size and also the fraction of intensity within this spot. Here, the focal spot size was measured to 151(3) nm and 156(3) nm for the uncorrected and corrected case, respectively. While being slightly larger than the theoretical value of 143 nm, no significant change was observed. On the other hand, due to the reduction of spherical aberration, side lobes in the focal plane were significantly reduced. The result is an increased concentration of photons within the central speckle of the focus, summarized by the relative speckle and on-axis intensity presented in Table 1.

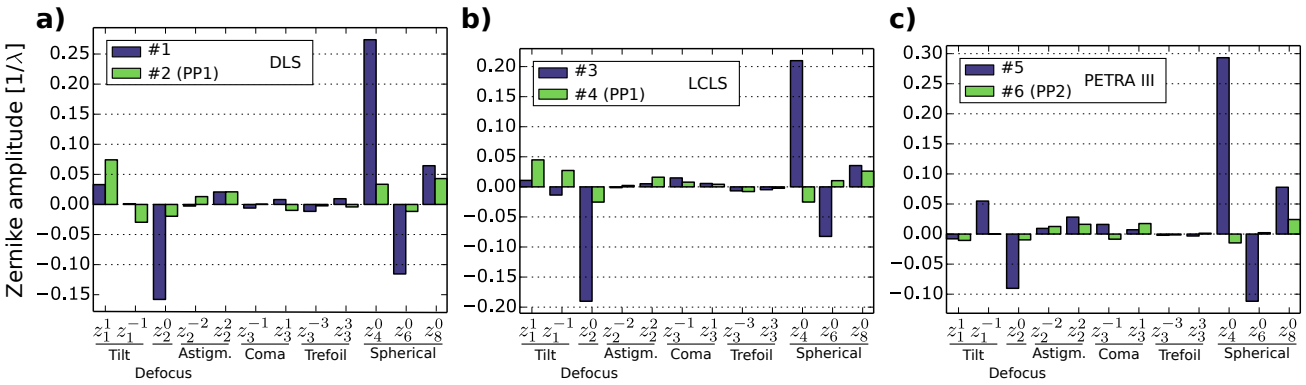

Figure 5. Strength of various aberrations represented by the Zernike amplitudes z_n^m. (a) Fit results for wavefields recovered at DLS (cf. Fig. 2a and Fig. 4a). (b) Fit results for wavefields recovered at LCLS (cf. Fig. 2b and Fig. 4b). (c) Fit results for wavefields recovered at PETRA III (cf. Fig. 2c and Fig. 4c).

6. CONCLUSIONS

We have demonstrated the correction of spherical aberration in three different Be CRL stacks at storage ring facilities and an XFEL. The relative on-axis intensity in the focal plane compared to an aberration-free optics, also known as the Strehl ratio,[33] was increased from 0.29(7) to 0.87(5) (cf. Table 1). Thus, we have demonstrated diffraction-limited focusing in the hard X-ray regime using radiation resistant, large aperture optics with $NA = 0.49 \times 10^{-3}$. With the increasing availability of XFELs operating in the hard X-ray regime and the advent of ultra-low emittance storage ring sources, the demand for suitable optics with high NA and ideally diffraction-limited performance is rising. The phase plate concept provides a compact and effective solution to correct refractive, diffractive, and reflective nanofocusing optics beyond current manufacturing limitations. Not only new focusing systems can benefit from increased performance, but in this way also existing optics can be upgraded for diffraction-limited focusing at the nanoscale.

ACKNOWLEDGMENTS

The authors thank Brice Arnold and Dirk Samberg for their technical support and Robert Hoppe for providing and maintaining the GPU-enhanced ptychographic engine. Parts of this research were carried out at the coherence branch of beamline I13 at Diamond Light Source (DLS) and beamline P06 at PETRA III at DESY, a member of the Helmholtz Association (HGF). Use of the Linac Coherent Light Source (LCLS), SLAC National Accelerator Laboratory, is supported by the US Department of Energy, Office of Science, Office of Basic Energy Sciences under Contract No. DE-AC02-76SF00515. The MEC instrument is supported by the US Department of Energy, Office of Science, Office of Fusion Energy Sciences under Contract No. SF00515. This work is supported by the German Ministry of Education and Research (BMBF) under Grant Number 05K13OD2 and the DFG under Grant SCHR 1137/1-1. F.S., A.S. and C.Rö. acknowledge a Peter Paul Ewald fellowship from the Volkswagen Foundation.

REFERENCES

[1] McNeil, B. W. J. and Thompson, N. R., "X-ray free-electron lasers," *Nat Photon* **4**, 814–821 (Dec. 2010).

[2] Hettel, R., "DLSR design and plans: an international overview," *Journal of Synchrotron Radiation* **21**, 843–855 (Sep 2014).

[3] Tamasaku, K., Shigemasa, E., Inubushi, Y., Katayama, T., Sawada, K., Yumoto, H., Ohashi, H., Mimura, H., Yabashi, M., Yamauchi, K., and Ishikawa, T., "X-ray two-photon absorption competing against single and sequential multiphoton processes," *Nat Photon* **8**, 313–316 (Apr. 2014).

[4] Schropp, A., Hoppe, R., Meier, V., Patommel, J., Seiboth, F., Ping, Y., Hicks, D. G., Beckwith, M. A., Collins, G. W., Higginbotham, A., Wark, J. S., Lee, H. J., Nagler, B., Galtier, E. C., Arnold, B., Zastrau,

U., Hastings, J. B., and Schroer, C. G., "Imaging shock waves in diamond with both high temporal and spatial resolution at an XFEL," *Sci. Rep.* **5**, 11089 (June 2015).

[5] Ayyer, K., Yefanov, O. M., Oberthür, D., Roy-Chowdhury, S., Galli, L., Mariani, V., Basu, S., Coe, J., Conrad, C. E., Fromme, R., Schaffer, A., Dörner, K., James, D., Kupitz, C., Metz, M., Nelson, G., Xavier, P. L., Beyerlein, K. R., Schmidt, M., Sarrou, I., Spence, J. C. H., Weierstall, U., White, T. A., Yang, J.-H., Zhao, Y., Liang, M., Aquila, A., Hunter, M. S., Robinson, J. S., Koglin, J. E., Boutet, S., Fromme, P., Barty, A., and Chapman, H. N., "Macromolecular diffractive imaging using imperfect crystals," *Nature* **530**, 202–206 (Feb. 2016).

[6] Morgan, A. J., Prasciolu, M., Andrejczuk, A., Krzywinski, J., Meents, A., Pennicard, D., Graafsma, H., Barty, A., Bean, R. J., Barthelmess, M., Oberthuer, D., Yefanov, O., Aquila, A., Chapman, H. N., and Bajt, S., "High numerical aperture multilayer Laue lenses," *Sci. Rep.* **5**, 9892 (June 2015).

[7] Patommel, J., Klare, S., Hoppe, R., Ritter, S., Samberg, D., Wittwer, F., Jahn, A., Richter, K., Wenzel, C., Bartha, J. W., Scholz, M., Seiboth, F., Boesenberg, U., Falkenberg, G., and Schroer, C. G., "Focusing hard x rays beyond the critical angle of total reflection by adiabatically focusing lenses," *Applied Physics Letters* **110**(10), 101103 (2017).

[8] Matsuyama, S., Emi, Y., Kino, H., Kohmura, Y., Yabashi, M., Ishikawa, T., and Yamauchi, K., "Achromatic and high-resolution full-field x-ray microscopy based on total-reflection mirrors," *Opt. Express* **23**, 9746–9752 (Apr 2015).

[9] Yumoto, H., Mimura, H., Koyama, T., Matsuyama, S., Tono, K., Togashi, T., Inubushi, Y., Sato, T., Tanaka, T., Kimura, T., Yokoyama, H., Kim, J., Sano, Y., Hachisu, Y., Yabashi, M., Ohashi, H., Ohmori, H., Ishikawa, T., and Yamauchi, K., "Focusing of X-ray free-electron laser pulses with reflective optics," *Nat Photon* **7**, 43–47 (Jan. 2013).

[10] Mimura, H., Yumoto, H., Matsuyama, S., Koyama, T., Tono, K., Inubushi, Y., Togashi, T., Sato, T., Kim, J., Fukui, R., Sano, Y., Yabashi, M., Ohashi, H., Ishikawa, T., and Yamauchi, K., "Generation of 10^{20} $\mathrm{W\,cm^{-2}}$ hard X-ray laser pulses with two-stage reflective focusing system," *Nat Commun* **5**, 3539 (Apr. 2014).

[11] Schropp, A., Hoppe, R., Meier, V., Patommel, J., Seiboth, F., Lee, H. J., Nagler, B., Galtier, E. C., Arnold, B., Zastrau, U., Hastings, J. B., Nilsson, D., Uhlén, F., Vogt, U., Hertz, H. M., and Schroer, C. G., "Full spatial characterization of a nanofocused x-ray free-electron laser beam by ptychographic imaging," *Sci. Rep.* **3**, 01633 (Apr. 2013).

[12] Seiboth, F., Schropp, A., Hoppe, R., Meier, V., Patommel, J., Lee, H. J., Nagler, B., Galtier, E. C., Arnold, B., Zastrau, U., Hastings, J. B., Nilsson, D., Uhlén, F., Vogt, U., Hertz, H. M., and Schroer, C. G., "Focusing XFEL SASE pulses by rotationally parabolic refractive x-ray lenses," *Journal of Physics: Conference Series* **499**(1), 012004 (2014).

[13] Rodenburg, J. M. and Faulkner, H. M. L., "A phase retrieval algorithm for shifting illumination," *Applied Physics Letters* **85**(20), 4795–4797 (2004).

[14] Thibault, P., Dierolf, M., Bunk, O., Menzel, A., and Pfeiffer, F., "Probe retrieval in ptychographic coherent diffractive imaging," *Ultramicroscopy* **109**(4), 338 – 343 (2008).

[15] Kewish, C. M., Thibault, P., Dierolf, M., Bunk, O., Menzel, A., Vila-Comamala, J., Jefimovs, K., and Pfeiffer, F., "Ptychographic characterization of the wavefield in the focus of reflective hard X-ray optics," *Ultramicroscopy* **110**(4), 325 – 329 (2010).

[16] Schropp, A., Boye, P., Feldkamp, J. M., Hoppe, R., Patommel, J., Samberg, D., Stephan, S., Giewekemeyer, K., Wilke, R. N., Salditt, T., Gulden, J., Mancuso, A. P., Vartanyants, I. A., Weckert, E., Schoder, S., Burghammer, M., and Schroer, C. G., "Hard x-ray nanobeam characterization by coherent diffraction microscopy," *Applied Physics Letters* **96**(9), 091102 (2010).

[17] Hönig, S., Hoppe, R., Patommel, J., Schropp, A., Stephan, S., Schöder, S., Burghammer, M., and Schroer, C. G., "Full optical characterization of coherent x-ray nanobeams by ptychographic imaging," *Opt. Express* **19**, 16324–16329 (Aug 2011).

[18] Kewish, C. M., Guizar-Sicairos, M., Liu, C., Qian, J., Shi, B., Benson, C., Khounsary, A. M., Vila-Comamala, J., Bunk, O., Fienup, J. R., Macrander, A. T., and Assoufid, L., "Reconstruction of an astigmatic hard X-ray beam and alignment of K-B mirrors from ptychographic coherent diffraction data," *Opt. Express* **18**, 23420–23427 (Oct 2010).

[19] Vila-Comamala, J., Diaz, A., Guizar-Sicairos, M., Mantion, A., Kewish, C. M., Menzel, A., Bunk, O., and David, C., "Characterization of high-resolution diffractive X-ray optics by ptychographic coherent diffractive imaging," *Opt. Express* **19**, 21333–21344 (Oct 2011).

[20] Schroer, C. G., Hönig, S., Goldschmidt, A., Hoppe, R., Patommel, J., Samberg, D., Schropp, A., Seiboth, F., Stephan, S., Schöder, S., Burghammer, M., Denecke, M., Wellenreuther, G., and Falkenberg, G., "Hard x-ray nano-beam characterization by ptychographic imaging," *Proc. SPIE* **8141**, 814103 (2011).

[21] Seiboth, F., Schropp, A., Scholz, M., Wittwer, F., Rödel, C., Wünsche, M., Ullsperger, T., Nolte, S., Rahomäki, J., Parfeniukas, K., Giakoumidis, S., Vogt, U., Wagner, U., Rau, C., Boesenberg, U., Garrevoet, J., Falkenberg, G., Galtier, E. C., Ja Lee, H., Nagler, B., and Schroer, C. G., "Perfect x-ray focusing via fitting corrective glasses to aberrated optics," *Nature Communications* **8**, 14623 (Mar. 2017).

[22] Rau, C., Wagner, U., Peach, A., Robinson, I. K., Singh, B., Wilkin, G., and Jones, C., "The diamond beamline i13l for imaging and coherence," *AIP Conference Proceedings* **1234**(1), 121–125 (2010).

[23] Nagler, B., Schropp, A., Galtier, E. C., Arnold, B., Brown, S. B., Fry, A., Gleason, A., Granados, E., Hashim, A., Hastings, J. B., Samberg, D., Seiboth, F., Tavella, F., Xing, Z., Lee, H. J., and Schroer, C. G., "The phase-contrast imaging instrument at the matter in extreme conditions endstation at lcls," *Review of Scientific Instruments* **87**(10) (2016).

[24] Schroer, C. G., Baumbach, C., Döhrmann, R., Klare, S., Hoppe, R., Kahnt, M., Patommel, J., Reinhardt, J., Ritter, S., Samberg, D., Scholz, M., Schropp, A., Seiboth, F., Seyrich, M., Wittwer, F., and Falkenberg, G., "Hard x-ray nanoprobe of beamline p06 at petra iii," *AIP Conference Proceedings* **1741**(1), 030007 (2016).

[25] Plackett, R., Horswell, I., Gimenez, E. N., Marchal, J., Omar, D., and Tartoni, N., "Merlin: a fast versatile readout system for medipix3," *Journal of Instrumentation* **8**(01), C01038 (2013).

[26] Pennicard, D., Lange, S., Smoljanin, S., Hirsemann, H., Graafsma, H., Epple, M., Zuvic, M., Lampert, M.-O., Fritzsch, T., and Rothermund, M., "The lambda photon-counting pixel detector," *Journal of Physics: Conference Series* **425**(6), 062010 (2013).

[27] Herrmann, S., Boutet, S., Duda, B., Fritz, D., Haller, G., Hart, P., Herbst, R., Kenney, C., Lemke, H., Messerschmidt, M., Pines, J., Robert, A., Sikorski, M., and Williams, G., "Cspad-140k: A versatile detector for lcls experiments," *Nuclear Instruments and Methods in Physics Research Section A: Accelerators, Spectrometers, Detectors and Associated Equipment* **718**, 550 – 553 (2013).

[28] Pelz, P. M., Guizar-Sicairos, M., Thibault, P., Johnson, I., Holler, M., and Menzel, A., "On-the-fly scans for x-ray ptychography," *Applied Physics Letters* **105**(25), 251101 (2014).

[29] Huang, X., Lauer, K., Clark, J. N., Xu, W., Nazaretski, E., Harder, R., Robinson, I. K., and Chu, Y. S., "Fly-scan ptychography," *Sci. Rep.* **5**, – (Mar. 2015).

[30] Deng, J., Nashed, Y. S. G., Chen, S., Phillips, N. W., Peterka, T., Ross, R., Vogt, S., Jacobsen, C., and Vine, D. J., "Continuous motion scan ptychography: characterization for increased speed in coherent x-ray imaging," *Opt. Express* **23**, 5438–5451 (Mar 2015).

[31] Maiden, A. M. and Rodenburg, J. M., "An improved ptychographical phase retrieval algorithm for diffractive imaging," *Ultramicroscopy* **109**(10), 1256 – 1262 (2009).

[32] Hoppe, R., Meier, V., Patommel, J., Seiboth, F., Lee, H. J., Nagler, B., Galtier, E. C., Arnold, B., Zastrau, U., Hastings, J., Nilsson, D., Uhlén, F., Voigt, U., Hertz, H. M., Schroer, C. G., and Schropp, A., "Full characterization of a focused wave field with sub 100 nm resolution," *Proc. SPIE* **8778**, 87780G (2013).

[33] van den Bos, A., "Aberration and the strehl ratio," *J. Opt. Soc. Am. A* **17**, 356–358 (Feb 2000).

[34] Uhlén, F., Rahomäki, J., Nilsson, D., Seiboth, F., Sanz, C., Wagner, U., Rau, C., Schroer, C. G., and Vogt, U., "Ronchi test for characterization of X-ray nanofocusing optics and beamlines," *Journal of Synchrotron Radiation* **21**, 1105–1109 (Sep 2014).

[35] Born, M. and Wolf, E., [*Principles of Optics: Electromagnetic Theory of Propagation, Interference and Diffraction of Light*], Pergamon Press (1980).

[36] Seiboth, F., Kahnt, M., Scholz, M., Seyrich, M., Wittwer, F., Garrevoet, J., Falkenberg, G., Schropp, A., and Schroer, C. G., "Quantitative characterization of aberrations in x-ray optics," *Proc. SPIE* **9963**, 99630P (2016).

[37] Chichkov, B. N., Momma, C., Nolte, S., von Alvensleben, F., and Tünnermann, A., "Femtosecond, picosecond and nanosecond laser ablation of solids," *Applied Physics A* **63**(2), 109–115 (1996).

[38] Joglekar, A., Liu, H., Spooner, G., Meyhöfer, E., Mourou, G., and Hunt, A., "A study of the deterministic character of optical damage by femtosecond laser pulses and applications to nanomachining," *Applied Physics B* **77**(1), 25–30 (2003).

[39] Nilsson, D., Uhlén, F., Holmberg, A., Hertz, H. M., Schropp, A., Patommel, J., Hoppe, R., Seiboth, F., Meier, V., Schroer, C. G., Galtier, E., Nagler, B., Lee, H. J., and Vogt, U., "Ronchi test for characterization of nanofocusing optics at a hard x-ray free-electron laser," *Opt. Lett.* **37**, 5046–5048 (Dec 2012).